GEOPHYSICS, VOL. 67, NO. 2 (MARCH-APRIL 2002); P. 484–491, 3 FIGS., 1 TABLE.
10.1190/1.1468608

Three-dimensional induction logging problems, Part 2: A finite-difference solution

Gregory A. Newman* and David L. Alumbaugh‡

ABSTRACT

A 3-D finite-difference solution is implemented for simulating induction log responses in the quasi-static limit that include the wellbore and bedding that exhibits transverse anisotropy. The finite-difference code uses a staggered grid to approximate a vector equation for the electric field. The resulting linear system of equations is solved to a predetermined error level using iterative Krylov subspace methods. To accelerate the solution at low induction numbers (LINs), a new preconditioner is developed. This new preconditioner splits the electric field into curl-free and divergence-free projections, which allows for the construction of an approximate inverse operator. Test examples show up to an order of magnitude increase in speed compared to a simple Jacobi preconditioner. Comparisons with analytical and mode matching solutions demonstrate the accuracy of the algorithm.

INTRODUCTION

Modeling induction log responses that include the wellbore, invasion, and bedding anisotropy is a nontrivial calculation requiring the 3-D solution of Maxwells's equations. Such 3-D simulations using the spectral Lanczos decomposition method (SLDM) are reported by Druskin et al. (1999) and van der Horst et al. (1999). A notable feature of the SLDM approach is its ability to obtain multifrequency responses very efficiently. Here, we investigate the finite-difference approach for solving 3-D induction logging problems. This method solves Maxwell's equations at a specific frequency by imposing a staggered grid on a second-order partial differential equation for the electric field. The resulting system is solved in an iterative manner to a given predetermined error level using Krylov subspace methods (see Newman and Alumbaugh, 1995; Alumbaugh et al., 1996). In our adaptation of the finite-difference scheme, we introduce a preconditioning technique that allows for a further acceleration in the calculations at low induction numbers, considerations for properly meshing the wellbore and invasion zones, and modifications to account for simple anisotropy in the vertical and horizontal bedding directions. This finite-difference solution is not intended to and cannot directly compete with the SLDM approach when multiple frequency responses are desired. For a single frequency, however, the method can be quite fast and is competitive with SLDM.

THE FINITE-DIFFERENCE METHOD

Isotropic formulation

Assuming a time-harmonic dependence of $e^{i\omega t}$, where $i = \sqrt{-1}$, a vector equation for the electric field for isotropic media can be derived from Maxwell's equations in the quasi-static limit. Following Newman and Alumbaugh (1995), we have

$$\nabla \times \nabla \times \mathbf{E} + i\omega\mu_o\sigma\,\mathbf{E} = -i\omega\mu_o\mathbf{J}. \tag{1}$$

In this equation, the electrical conductivity σ is assumed to be isotropic; treatment for conductive media exhibiting transverse anisotropy are given in Appendix A. Here the free-space magnetic permeability and angular frequencies are denoted by μ_o and ω. Specification of the source vector $\mathbf{J}$ depends on whether a total or scattered electric-field solution is desired. In well-logging applications, we prefer a scattered-field formulation because measurements are often made very near the source. In this situation, our experience has shown that a total-field solution requires very fine meshing. This leads to large demands on computational resources, and it is virtually impossible to obtain accurate in-phase responses after the direct-coupled field has been removed. In a scattered-field formulation, we would set $\mathbf{E} = \mathbf{E}^s$ in equation (1) and, following Newman and Alumbaugh (1995), would set

$$\mathbf{J} = (\sigma - \sigma_b)\mathbf{E}^b, \tag{2}$$

Manuscript received by the Editor November 1, 2000; revised manuscript received July 2, 2001.
*Sandia National Laboratories, MS 0750, 1515 Eubank SE, Albuquerque, New Mexico 87185-0750. E-mail: ganewma@sandia.gov.
‡University Wisconsin–Madison, Department of Civil and Environmental Engineering, 2258 Engineering Hall, 1451 Engineering Dr., Madison, Wisconsin 53706. E-mail: alumbaugh@engr.wisc.edu.

where σ_b is the background conductivity of a uniform medium and $\mathbf{E}^b$ is the background electric field. For highly accurate results in induction logging applications, we have found that specification of the background medium should be based on the formation properties nearest the transmitter when it is isotropic. For anisotropic media, however, proper selection of the background medium is still an open research question; this issue is explored further in Avdeev et al. (2002).

When equation (1) is approximated with finite differences using a Yee (1966) staggered grid, symmetrically scaled, and Dirichlet boundary conditions applied (cf. Newman and Alumbaugh, 1995; Alumbaugh et al., 1996), a linear system results, where

$$\mathbf{KE} = \mathbf{S}. \tag{3}$$

The matrix $\mathbf{K}$ is complex symmetric and sparse with a maximum of 13 nonzero entries per row; $\mathbf{S}$ is a discrete and scaled representation of $\mathbf{J}$. This system can be solved efficiently at moderate to high frequencies using the quasi-minimum residual method with simple Jacobi preconditioning. Solution treatment as frequencies approach the static limit are discussed below. The quasi-minimum residual method belongs to the class of Krylov subspace techniques that are highly efficient in iteratively solving sparse linear systems to a predetermined error level. [Refer to Newman and Alumbaugh (1995) and Alumbaugh et al. (1996) for details on how these solvers are implemented.] Once the electric field is determined from equation (3), the magnetic field is determined from Faraday's law by numerically approximating the curl of the electric field at the various nodal points and interpolating either the electric or magnetic nodal values to the point of interest. If the solution of equation (3) produces scattered fields, then background electric and magnetic fields must be added to the interpolated fields to yield the total fields.

PRECONDITIONING

It is well known that, when attempting to solve equation (3), difficulties will be encountered as frequencies approach the static limit (Alumbaugh et al., 1996; Smith, 1996). Similar difficulties are reported by Druskin et al., (1999) when equation (1) is solved with SLDM, which also uses finite-difference approximations. In this section, we show how these difficulties can be overcome with preconditioning. The preconditioner we introduce parallels the work of Druskin et al. (1999), who developed an SLDM method with Krylov subspaces generated from the inverse of the Maxwell operator.

Following LaBrecque (1999) and Druskin et al. (1999), we assume that the electric field can be decomposed into curl-free and divergence-free projections using the Helmholtz theorem, where

$$\mathbf{E} = \mathbf{\Psi} + \nabla\varphi \tag{4}$$

and

$$\nabla \cdot \mathbf{\Psi} = 0. \tag{5}$$

Substituting equations (4) and (5) into equation (1), we find that

$$-\nabla^2\mathbf{\Psi} + i\omega\mu_o\sigma(\mathbf{\Psi} + \nabla\varphi) = -i\omega\mu_o\mathbf{J}, \tag{6}$$

where we use the vector identity

$$\nabla\times\nabla\times\mathbf{\Psi} = -\nabla^2\mathbf{\Psi} \tag{7}$$

since $\nabla\times\nabla\times\nabla\varphi = 0$. The idea behind splitting the electric field into curl-free and divergence-free projections is to deflate the null space of the curl–curl operator. When Krylov methods are applied directly to equation (1), this null space is responsible for the poor convergence observed in the solution of equation (3) as the frequency approaches the static limit. It is also responsible for the spurious mode problem, where the gradient of a scalar potential can be added to the electric field and still satisfy the discrete version of equation (1) when the frequency is sufficiently small.

We now seek to develop an approximate finite-difference solution to equation (6) at low frequencies. To this end we need to estimate the relative sizes of the curl–curl and attenuation operators in equation (1). Assuming a finite-difference approximation, where Δ is the characteristic grid size in the finite-difference mesh, the curl–curl operator is estimated to be roughly $1/\Delta^2$; the attenuation operator is $\omega\mu_o\sigma_{max}$. Here, σ_{max} is the maximum conductivity in the mesh. Thus, as frequency falls and the grid size is reduced, we observe the condition

$$1/\Delta^2 \gg \omega\mu_o\sigma_{max} \tag{8}$$

or

$$1 \gg \Delta^2\omega\mu_o\sigma_{max}. \tag{9}$$

When the finite-difference grid is nonuniform, Δ should be replaced by Δ_{max}, the maximum grid size used to approximate equation (1). Note that the right-hand side of equation (9) is a dimensionless number and its square root is an induction number, which is an invariant parameter for diffusive electromagnetic fields. When frequency falls, we increase the scale length and/or conductivity accordingly to have the fields remain invariant. Thus, the induction number appears to be more important in determining when equation (9) holds than frequency alone. Also, even at moderate frequencies, equation (9) may still hold if the grid size needed for the problem is sufficiently small. This has direct implications for induction logging problems which use small grid sizes. Now, if equation (9) is satisfied, we can decouple equation (6) such that

$$-\nabla^2\mathbf{\Psi} \approx -i\omega\mu_o\mathbf{J}. \tag{10}$$

The boundary conditions required to solve equation (10) are a mixture of Dirichlet and Neumann types. Dirichlet conditions are applied to the tangential components of $\mathbf{\Psi}$ on the mesh boundaries, $\mathbf{\Psi}_t = 0$, and Neumann conditions on the normal components, $\partial\mathbf{\Psi}_n/\partial n = 0$. These conditions enforce the requirement that $\nabla\cdot\mathbf{\Psi} = 0$ on the mesh boundaries and in turn within the solution domain, since the divergence-free field is required to satisfy the constraint equation

$$\nabla^2(\nabla\cdot\mathbf{\Psi}) = 0. \tag{11}$$

Equation (11) follows by applying the divergence operator to equation (7). It is well known that when a function u satisfies Laplace's equation, $\nabla^2 u = 0$, on some domain Ω with homogeneous boundary conditions of $u = 0$ or $\partial u/\partial n = 0$ prescribed along the boundary Γ, it is identically zero on that domain. Note

that when applying the Neumann boundary condition, n would specify the direction of the outward normal at the boundary.

The vector field Ψ is not a complete solution to Maxwell's equations since it does not satisfy the auxiliary divergence condition on the current density within the earth. To derive this condition, we take the divergence of equation (1) and substitute equation (4) to arrive at

$$\nabla \cdot \sigma(\nabla\varphi) = -\nabla \cdot \sigma(\Psi) - \nabla \cdot \mathbf{J}. \tag{12}$$

Dirichlet boundary conditions will be applied to the discrete version of equation (12), where $\varphi = 0$ on the mesh boundaries. When the air–earth interface is present, however, we use the Neumann condition, $\partial\varphi/\partial n = 0$, where n specifies the direction of the outward normal at that interface. This later boundary condition enforces the constraint that current cannot leak from the earth into the air.

Thus, approximate solutions of equation (6) at very small induction numbers can be obtained by first solving equation (10), followed by equation (12). A solution to these equations can be obtained efficiently using staggered finite-difference methods with conjugate-gradient methods to iteratively solve the systems to predetermined error levels.

Now if it turns out that we cannot obtain a good approximate solution to equation (3) with a reasonable number of Krylov subspace iterations or if such an approximate solution cannot be easily computed, we consider modifying the original problem to obtain a faster solution. This is the idea behind preconditioning, where we specify a preconditioning matrix $\mathbf{M}$ and effectively solve the modified problem

$$\mathbf{M}^{-1}\mathbf{KE} = \mathbf{M}^{-1}\mathbf{S}. \tag{13}$$

At each step of the preconditioned algorithm, it is necessary to compute the product of $\mathbf{M}^{-1}$ with a vector, or equivalently to solve a linear system with the coefficient matrix $\mathbf{M}$; so $\mathbf{M}$ should be chosen such that this linear system is much easier to solve than the original problem. Moreover, the properties we desire in a preconditioner for non-Hermitian matrix iterations, including quasi-minimum residual and other related methods, are that the preconditioned matrix should somehow approximate the identity matrix (Greenbaum, 1997). It is therefore obvious that the approximate scheme discussed above could be very effective in preconditioning equation (3) at moderate to low induction numbers (LINs). If this idea is to be practical, however, we must find fast methods to solve the approximate equations. A good preconditioner is not simply based on a relatively low-dimension Krylov subspace but on the time required to construct it. In the implementation of the LIN preconditioner, we first convert equations (10) and (12) into discrete matrix equations via staggered finite differences. In the preconditioned quasi-minimum residual algorithm, at each iteration, we then substitute the residual, defined by $\mathbf{r} = \mathbf{KE} - \mathbf{S}$, into the right-hand side of the discrete version of equation (10). Equation (10) is then solved, followed by equation (12). Fast preconditioned conjugate gradient techniques employing incomplete Cholesky factorization have proven to be quite effective when solving these equations. Furthermore, we have determined that it is not necessary to precisely solve these equations. Test examples show that we only need to approximately solve these equations for a significant impact on reducing the time required for solving equation (3).

Equation (9) provides only a rough measure on the effectiveness of the preconditioner. For a better measure we need to estimate the largest and smallest nonzero values that the discrete curl–curl operator can assume. This naturally leads to estimating its eigenvalues, which is useful in determining when the preconditioner will be the most and the least effective. Consider equation (3) when $\omega = 0$. Using the maximum row sum, we find the largest eigenvalue of the discrete curl–curl operator satisfies

$$\lambda_{max} \approx \frac{13}{\Delta_{min}^2}, \tag{14}$$

where Δ_{min} is the minimum grid size used in the mesh. The corresponding minimum nonzero eigenvalue is estimated in Appendix B, where

$$\lambda_{min} \approx \frac{2\pi^2}{L_{max}^2}, \tag{15}$$

with L_{max} as the largest dimension of the 3-D Cartesian mesh. Given the largest eigenvalue estimate, the inequality in equation (9) is written as

$$1 \gg \frac{\omega\mu_o\sigma_{max}\Delta_{min}^2}{13}, \tag{16}$$

which provides an optimistic measure when the preconditioner will be most effective. In the worst case, however, which corresponds to the smallest nonzero eigenvalue, we have

$$1 \gg \frac{\omega\mu_o\sigma_{max}L_{max}^2}{2\pi^2}. \tag{17}$$

Unfortunately, equation (17) shows that reducing the grid size Δ does not solve equation (3) faster. It is well known that Krylov methods tend to first resolve solution components related to eigenvectors with the largest eigenvalues of the matrix $\mathbf{K}$. As frequency falls or at small induction numbers, these eigenvalues correspond closely to those of the curl–curl operator. If only the larger eigenvalues are needed to produce an accurate solution to the problem, then the inequality in equation (16) would provide a good measure of the effectiveness of the preconditioner. On the other hand, if eigenvectors corresponding to the smaller eigenvalues are necessary to capture the solution, then equation (17) would provide a better measure.

Mesh considerations

To simulate induction log responses with the finite-difference scheme, we need to approximate the cylindrical borehole, including any invasion zones, using a Cartesian grid. In induction logging simulations, this approximation yields satisfactory results if the borehole/invasion-zone diameter is small compared to the wavelengths excited in the media. This is almost always the case, given the frequencies typically used in logging applications are <50 MHz and the electrical conductivity of drilling mud and rocks are <20 S/m (Hohmann and Ward, 1988). Figure 1 shows how the Cartesian grid is imposed upon the problem where the borehole deviates 45° from the vertical. In horizontal cross-section the borehole appears elliptical in shape, and the conductivity of the cells that intersect the borehole boundary are assigned by averaging the conductivity of the drilling mud and formation according to that proportion

of the cell volume intersecting the different media. In vertical cross-section, the grid results in a staircasing of the borehole. Nevertheless, we have determined through numerical experiments, as demonstrated below, that the Cartesian grid works quite well and can produce simulation results accurate to within a few percent, provided the cell size over the borehole volume does not exceed a few centimeters. Finally, it is only necessary to impose the grid on half of the problem because of symmetry; note that the tangential electric fields vanish along the symmetry plane ($y = 0$) when coaxial magnetic sources are deployed. It is also possible to use symmetry when the source is off axis of the borehole. The requirements are that the source be located on the symmetry plane with a magnetic moment parallel to the plane of symmetry.

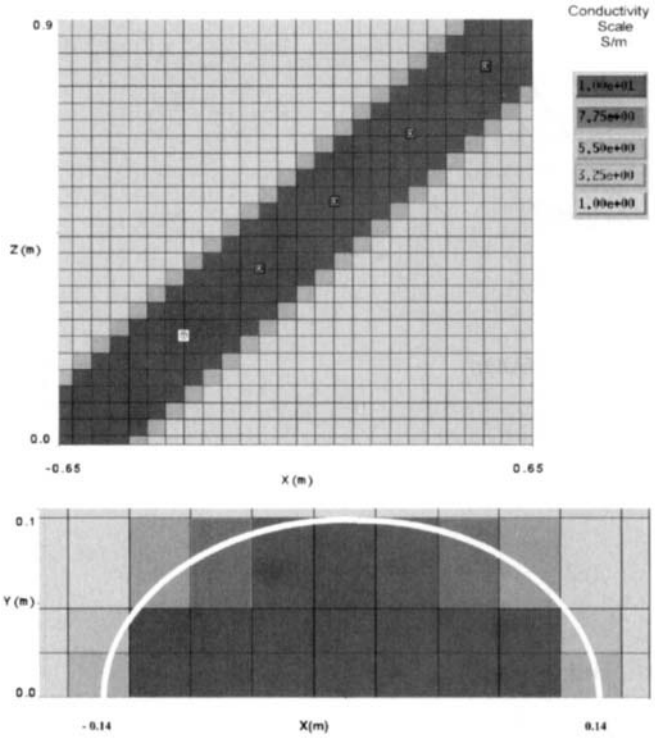

FIG. 1. Finite-difference discretization of a cylindrical borehole deviating 45° using a Cartesian grid (top). The mesh in the vertical cross-section (bottom). The mesh in the horizontal cross-section is for half of the borehole and surrounding formation. A semiellipse in the lower panel indicates the true shape of the borehole in the horizontal cross-section. The grayscale to the right provides the range of conductivities used in the mesh.

DEMONSTRATION OF THE FINITE-DIFFERENCE SOLUTION

Effectiveness of the LIN preconditioner

We now demonstrate through a self-consistency check the ability of the finite-difference solution to simulate deviated borehole responses and demonstrate the effectiveness of the LIN preconditioner. Consider a 45° deviated borehole as shown in Figure 2a, where the mud resistivity is 0.05 ohm-m and the formation is 50 ohm-m. The radius of the wellbore is 10 cm, where the transmitter–receiver offsets range from 0.2 to 4 m (offsets beyond 2 m are not shown in Figure 2a). The transmitter is a magnetic dipole, coaxial with the borehole, and the receivers sample the coaxial magnetic field at 160 kHz. The mesh consists of 134 832 grid points that sample 337 376 electric-field unknowns on a domain that is $16 \times 6 \times 16$ m in the x, y, and z coordinate directions. Figure 2b illustrates the convergence rate of the finite-difference solution when simple Jacobi preconditioning is used, where the solution time is 1672 s for an IBM RS-6000 590 workstation. When the problem is solved using the LIN preconditioner, the solution time is 187 s—nearly an order of magnitude faster. To verify the finite-difference responses for this model, we compare the responses in Figure 2c to the mode matching solution of Chew et al. (1984). Excellent agreement is observed over the complete range of offsets. In these comparisons, we have not removed the direct-coupled field in the real (in-phase) responses; hence, the real values of the field are greater than the quadrature values. Finite-difference responses, where the direct-coupled field has been removed, are presented below and in the companion modeling paper (Avdeev et al., 2002), where excellent results are also reported.

Table 1 shows the effectiveness of the LIN preconditioner over three decades of frequency. As expected, the preconditioner is most effective at lower frequencies. For the highest frequency, 5 MHz, the preconditioner can actually fail to converge and may also result in much slower solution times than a solution that uses simple Jacobi preconditioning. In this example, the upper bound given by equation (16) provides a good measure of when to use the LIN precondioner, provided the right-hand side of equation (16) is at least two orders of magnitude smaller than its left-hand side. The lower bound expression [equation (17)], on the other hand, is too pessimistic.

Table 1. LIN preconditioner effectiveness over three decades of frequency. The model from which the table is constructed is shown in Figure 2. The squared residual norm, $\|\mathbf{KE} - \mathbf{S}\|^2/\|\mathbf{S}\|^2$, terminates the solution iteration process and is based on a threshold value of 1.0e-08. When a simulation could not achieve this threshold, the solution iteration was terminated at 30 quasi-minimum residual iterations. Values based on the right sides of equations (16) and (17) are also included in the table and help estimate when the preconditioner will be effective before the quasi-minimum residual solution is attempted.

Frequency	Solution time (s)	Iterations	Squared residual norm	Equation (16)	Equation (17)
10 kHz	148	3	2e-09	3.0e-04	20.5
40 kHz	185	4	5e-11	1.2e-03	82
80 kHz	184	4	1.5e-10	2.4e-03	164
160 kHz	187	4	1.8e-10	4.8e-03	328
320 kHz	191	4	8.9e-10	9.6e-03	656
640 kHz	229	5	4.2e-09	1.9e-02	1312
1 MHz	316	7	7.7e-09	3.0e-02	2050
5 MHz	1251	30	1.4e-07	1.5e-01	10 250

Additional examples demonstrating the LIN preconditioner on more complex induction models can be found in Avdeev et al. (2001, Table 2). The examples show the LIN preconditioner can be very effective for frequencies as high as 160 kHz and can produce a solution up to about five times faster than a solution using Jacobi preconditioning.

CONCLUSIONS

A finite-difference solution has been developed for simulating 3-D induction logging responses. Important features of the solution include a novel preconditioner that can significantly reduce computation times at low induction numbers and frequencies and the incorporation of transverse anisotropy into the solution. Furthermore, measures have been derived to indicate when the preconditioner will be effective. The solution is quite general and is capable of simulating borehole effects as well. In the companion paper of Avdeev et al. (2002), we compare this solution to an iterative integral equation solution for 3-D induction logging problems in deviated boreholes with anisotropic bedding.

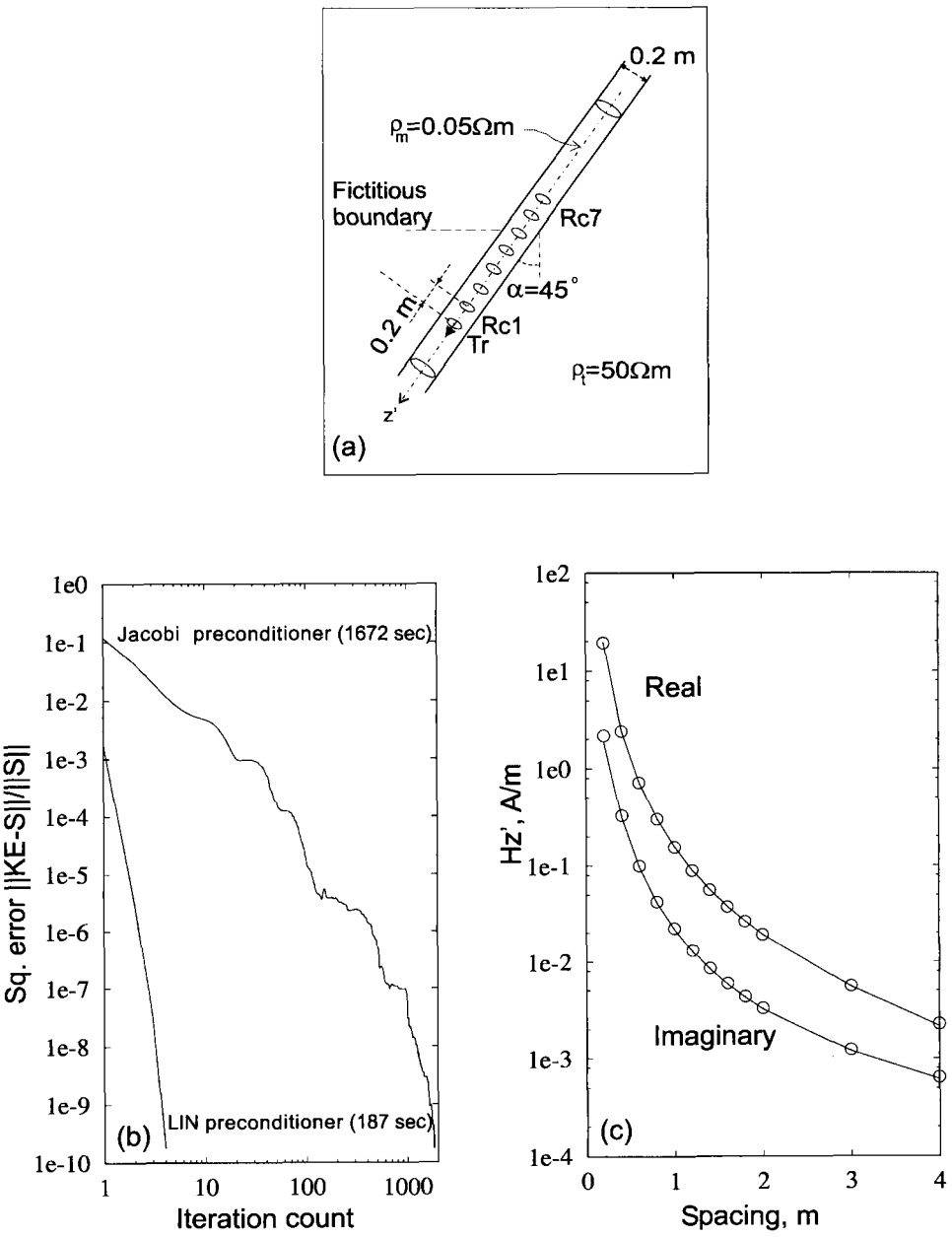

FIG. 2. Comparison and self-constancy check of the finite-difference solution for a 45° deviated borehole within a uniform background medium of 50 ohm-m. (a) The borehole diameter is 20 cm, and mud resistivity is 0.05 ohm-m. The transmitter-receivers span offsets ranging from 0.2 to 4 m. (b) The convergence rate of the finite-difference solution for Jacobi and LIN preconditioning at 160 kHz along with the required computation times. (c) Finite-difference responses (solid-lines) compared to the mode-matching solution (small circles) of Chew et al. (1984).

ACKNOWLEDGMENTS

The authors recognize the assistance of David Day and Louis Romero of Sandia National Laboratories in the development of measures to gauge the effectiveness of the LIN preconditioner. This work was performed at Sandia National Laboratories, with funding provided by the Sandia National Laboratories Industrial Partnership Program (IPP), sponsored by the U.S. Department of Energy (DOE) and the DOE Oil Technology Partnership Program. Sandia National Laboratories is a multiprogram laboratory operated by the Sandia Corporation, a Lockheed Martin Company, for the U.S. DOE under contract DE-AC04-94AL85000.

REFERENCES

Alumbaugh, D. L., Newman, G. A., Prevost, L., and Shadid, J., 1996, Three-dimensional wideband electromagnetic modeling on massively parallel computers: Radio Sci., **31**, 1–23.

Avdeev, D. B., Kuvshinov, A. V., Pankratov, O. V., and Newman, G. A., 2002, Three-dimensional induction logging problems, Part 1: An integral equation solution and model comparisons: I: Geophysics, **67**, 413–426.

Chew, W. C., Barone, S., Anderson, B., and Hennessy, C., 1984, Diffraction of axisymmetric waves in a borehole by bed boundary discontinuities: Geophysics, **49**, 1586–1595.

Druskin, V., Knizhnerman, L., and Lee, P., 1999, A new spectral Lanczos decomposition method for induction modeling in arbitrary 3-D geometry: Geophysics, **64**, 701–706.

Greenbaum, A., 1997, Iterative methods for solving linear systems: Soc. Indust. Appl. Math.

Hohmann, G. W., and Ward, S. H., 1988, Electromagnetic theory for geophysical applications: Soc. Expl. Geophys.

LaBrecque, D., 1999, Finite difference modeling of 3-D EM fields with scalar and vector potentials, *in* Oristaglio, M., and Spies, B., Eds., Three-dimensional electromagnetics: Soc. Expl. Geophys., 148–160.

Newman, G. A., and Alumbaugh, D. L., 1995, Frequency-domain modeling of airborne electromagnetic responses using staggered finite differences: Geophys. Prosp., **43**, 1021–1042.

Smith, J. T., 1996, Conservative modeling of 3-D electromagnetic fields, Part II: Biconjugate gradient solution and an accelerator: Geophysics, **61**, 1319–1324.

van der Horst, M., Druskin, V., and Knizhnerman, L., 1999, Modeling induction logs in 3-D geometries, *in* Oristaglio, M., and Spies, B., Ed., Three-dimensional electromagnetics: Soc. Expl. Geophys., 611–622.

Yee, K. S., 1966, Numerical solution of the initial boundary value problems involving Maxwell's equations in isotropic media: IEEE Trans. Antennas Prop., **AP-14**, 302–309.

APPENDIX A
SOLUTION TREATMENT FOR TRANSVERSE ANISOTROPIC MEDIA

The electromagnetic staggered finite-difference method for transverse anisotropic conductive media is a simple extension of the scattered-field version of equation (1), where

$$\nabla\times\nabla\times\mathbf{E}^s(\mathbf{r}) + i\omega\mu_o\boldsymbol{\sigma}(\mathbf{r})\mathbf{E}^s(\mathbf{r}) = -i\omega\mu_o(\boldsymbol{\sigma}(\mathbf{r}) - \sigma_b(\mathbf{r}))\mathbf{E}^b(\mathbf{r}). \quad \text{(A-1)}$$

Here $\mathbf{E}^s(\mathbf{r})$ is the scattered electric field, $\sigma_b(\mathbf{r})$ is the background electrical conductivity, and $\mathbf{E}^b(\mathbf{r})$ is the electric field of the background medium. In our case $\sigma_b(\mathbf{r})$ is assumed to be an isotropic whole space (i.e., $\sigma_b(\mathbf{r}) = \sigma^{ws}$); thus, $\mathbf{E}^b(\mathbf{r})$ can be calculated analytically.

The fundamental difference between this expression and that given in equation (1) and in Newman and Alumbaugh (1995) is that $\boldsymbol{\sigma}(\mathbf{r})$ is now a 3×3 tensor that represents the anisotropic conductivity. In the most general case this tensor is full. However, in the case of transverse anisotropy only the main diagonal is nonzero, i.e.,

$$\boldsymbol{\sigma}(\mathbf{r}) = \begin{bmatrix} \sigma_{xx}(\mathbf{r}) & 0 & 0 \\ 0 & \sigma_{yy}(\mathbf{r}) & 0 \\ 0 & 0 & \sigma_{zz}(\mathbf{r}) \end{bmatrix}, \quad \text{(A-2)}$$

where $\sigma_{xx}(\mathbf{r})$ is the electrical conductivity in the $\hat{\mathbf{x}}$ direction, $\sigma_{yy}(\mathbf{r})$ is the electrical conductivity in the $\hat{\mathbf{y}}$ direction, and $\sigma_{zz}(\mathbf{r})$ is the electrical conductivity in the $\hat{\mathbf{z}}$ direction.

Combining equation (A-2) with (A-1) and expanding the curl operations yields the following three coupled expressions for the scattered electric fields:

$$\frac{\partial}{\partial y}\left(\frac{\partial E_y^s(\mathbf{r})}{\partial x} - \frac{\partial E_x^s(\mathbf{r})}{\partial y}\right) - \frac{\partial}{\partial z}\left(\frac{\partial E_x^s(\mathbf{r})}{\partial z} - \frac{\partial E_z^s(\mathbf{r})}{\partial x}\right) + i\omega\mu_0\sigma_{xx}(\mathbf{r})E_x^s(\mathbf{r}) = -i\omega\mu_0(\sigma_{xx}(\mathbf{r}) - \sigma^{ws})E_x^b(\mathbf{r}), \quad \text{(A-3)}$$

$$\frac{\partial}{\partial z}\left(\frac{\partial E_z^s(\mathbf{r})}{\partial y} - \frac{\partial E_y^s(\mathbf{r})}{\partial z}\right) - \frac{\partial}{\partial x}\left(\frac{\partial E_y^s(\mathbf{r})}{\partial x} - \frac{\partial E_x^s(\mathbf{r})}{\partial y}\right) + i\omega\mu_0\sigma_{yy}(\mathbf{r})E_y^s(\mathbf{r}) = -i\omega\mu_0(\sigma_{yy}(\mathbf{r}) - \sigma^{ws})E_y^b(\mathbf{r}), \quad \text{(A-4)}$$

and

$$\frac{\partial}{\partial x}\left(\frac{\partial E_x^s(\mathbf{r})}{\partial z} - \frac{\partial E_z^s(\mathbf{r})}{\partial x}\right) - \frac{\partial}{\partial y}\left(\frac{\partial E_z^s(\mathbf{r})}{\partial y} - \frac{\partial E_y^s(\mathbf{r})}{\partial z}\right) + i\omega\mu_0\sigma_{zz}(\mathbf{r})E_z^s(\mathbf{r}) = -i\omega\mu_0(\sigma_{zz}(\mathbf{r}) - \sigma^{ws})E_z^b(\mathbf{r}). \quad \text{(A-5)}$$

Each equation contains a different component of the conductivity tensor, and the equations are not cross-coupled in terms of the directional conductivities. When expressions (A-3)–(A-5) are expanded numerically using the staggered finite-difference operator of Yee (1966), the terms containing the variable electrical conductivity are confined to the main diagonal of the sparse stiffness matrix and to the source vector. Thus, the equations defining the problem are identical in structure to those given in Newman and Alumbaugh (1995, Appendix A), which results in a stiffness matrix that is complex symmetric. This system of equations can therefore be solved using the same methods as the isotropic solution. [See Newman and Alumbaugh (1995) for details on how this is done.]

As an additional note, in transverse anisotropic media we often assume that the electrical conductivity is constant parallel to the bedding. Thus, if the bedding is assumed to be horizontal, the conductivity tensor can be further simplified to read

$$\boldsymbol{\sigma}(\mathbf{r}) = \begin{bmatrix} \sigma_h(\mathbf{r}) & 0 & 0 \\ 0 & \sigma_h(\mathbf{r}) & 0 \\ 0 & 0 & \sigma_v(\mathbf{r}) \end{bmatrix}. \quad \text{(A-6)}$$

Here, $\sigma_h(\mathbf{r})$ represents the electrical conductivity in the horizontal direction, i.e., parallel to the bedding, and $\sigma_v(\mathbf{r})$ is the conductivity perpendicular to the beds.

To verify the finite-differences solution to simulate responses arising from anisotropic media, we consider a whole-space model with vertical and transverse resistivities of 1 and 4 ohm-m (Figure A-1a). The point magnetic dipole transmitter and receivers are deviated 45° from the vertical. Because of the deviation in the transmitter, electric currents are induced to flow in both the transverse and vertical directions, exciting a magnetic-field response sensitive to the vertical and transverse resistivities of the medium. Figure A-1b compares the finite-difference results (in-phase and quadrature responses) to those produced using a 1-D fast Hankel transform. The comparison is excellent.

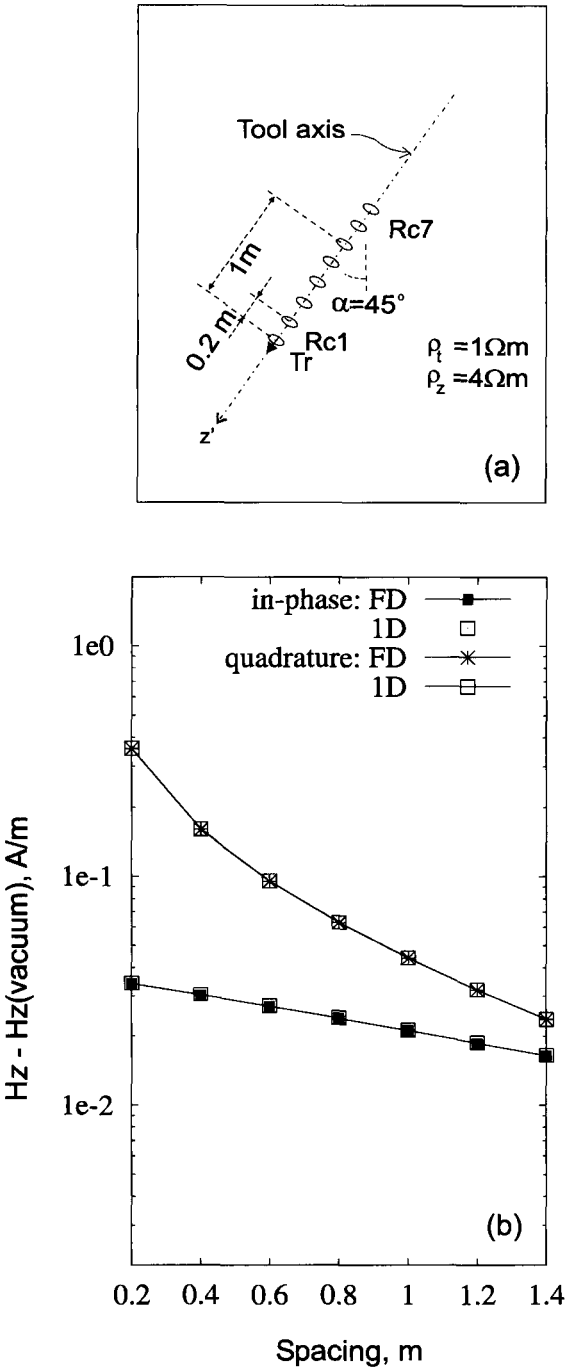

FIG. A-1. Comparison of the finite-difference results (crosses and vertical dash symbols) with those produced from a 1-D fast Hankel transform solution (solid lines) for a transversely anisotropic whole-space model at (a) 160 kHz. (b) Real (in-phase) and quadrature comparisons. The direct-coupled field has been removed from the real responses.

APPENDIX B
SMALLEST NONZERO EIGENVALUE ANALYSIS

To estimate the smallest nonzero eigenvalue of the matrix **K** in equation (3) when $\omega = 0$, we first consider the curl–curl operator in the continuous case. Thus,

$$\nabla \times \nabla \times \mathbf{v} = \lambda \mathbf{v}, \tag{B-1}$$

where **v** and λ are the corresponding eigenvector and eigenvalue pairs. If we apply the divergence operator to equation (B-1), we immediately see that

$$0 = \lambda \nabla \cdot \mathbf{v}. \tag{B-2}$$

Since we are interested in the case where $\lambda \neq 0$, we conclude that

$$\nabla \cdot \mathbf{v} = 0. \tag{B-3}$$

Thus, the eigenvalue problem can be simplified to

$$-\nabla^2 \mathbf{v} = \lambda \mathbf{v}, \tag{B-4}$$

where we seek solutions to this problem under the constraint that **v** is divergence free. When we consider the discrete case, we need to impose boundary conditions on **v**, where its tangential components vanish on the boundaries of the modeling grid. Specifically,

$$\mathbf{n} \cdot \mathbf{v} = \mathbf{0}, \tag{B-5}$$

where **n** is the unit outward normal. We also require that the normal derivatives of **v** vanish on the boundaries. These boundary conditions are required to ensure that **v** is divergence free. Candidate eigenfunctions that satisfy these boundary condition requirements are

$$\begin{aligned} v_x &= A \cos(\alpha x) \sin(\beta y) \sin(\delta z), \\ v_y &= B \sin(\alpha x) \cos(\beta y) \sin(\delta z), \end{aligned} \tag{B-6}$$

and

$$v_z = C \sin(\alpha x) \sin(\beta y) \cos(\delta z),$$

where $\alpha = \pi / L_x$, $\beta = \pi / L_y$, and $\delta = \pi / L_z$, and where L_x, L_y, and L_z are the dimensions of the modeling domain in the x, y, and z directions. The coefficients A, B, and C are not arbitrary in equation (B-6) because $\nabla \cdot \mathbf{v} = 0$. Thus, once two components of **v** are specified, the final component must be selected such that **v** is divergence free. For example, if $A = \beta\delta$ and $B = \alpha\delta$, then $C = -2\alpha\beta$.

If we consider the discrete version of equation (B-4) on a mesh with uniform grid size Δ, we can show with equation (B-6) that

$$\lambda = \frac{4}{\Delta^2}\left(\sin^2\left(\frac{l\pi\Delta}{2L_x}\right) + \sin^2\left(\frac{m\pi\Delta}{2L_y}\right) + \sin^2\left(\frac{n\pi\Delta}{2L_z}\right)\right). \tag{B-7}$$

The range on the indices l, m, and n range as follows: $l = 0, 1, \ldots, N_x$; $m = 0, 1, \ldots, N_y$; and $n = 0, 1, \ldots, N_z$, where $L_x = \Delta N_x$, $L_y = \Delta N_y$ and $L_z = \Delta N_z$. To estimate the smallest nonzero value of λ, we set L_x, L_y, and L_z to the largest dimension of the modeling domain, L_{max}. If we select l, m, or n to be zero and the others to be one (we arbitrarily set $l = 0$, $m = 1$, and $n = 1$) and employ a small argument expression for the sine function ($\sin(x) \approx x$ when $x \to 0$), we find an estimate of the smallest nonzero eigenvalue to be

$$\lambda_{min} \approx \frac{2\pi^2}{L_{max}^2}. \tag{B-8}$$

Note that we cannot set two of the indices to be zero in equation (B-7) because this would result in a zero eigenvector, which is a trivial solution to the eigenvalue problem.